ORIGINAL PAPER

RJME
Romanian Journal of Morphology & Embryology
http://www.rjme.ro/

Eu^{3+}-doped ZnO nanostructures: advanced characterizations, photoluminescence and cytotoxic effect

BOGDAN ŞTEFAN VASILE, OTILIA RUXANDRA VASILE, DANIELA CRISTINA GHIŢULICĂ, FLORINA CRISTINA ILIE, IRINA FLORENTINA NICOARĂ, ROXANA TRUŞCĂ, OVIDIU CRISTIAN OPREA, VASILE ADRIAN SURDU, IONELA ANDREEA NEACŞU

Faculty of Applied Chemistry and Materials Science, Politehnica University of Bucharest, Romania
National Centre for Micro and Nanomaterials, Politehnica University of Bucharest, Romania
National Research Center for Food Safety, Politehnica University of Bucharest, Romania

Abstract

In this work, several nanostructures (nanopowders and nanostars) of undoped and 1%, 3% and 5% europium (Eu^{3+})-doped ZnO have been synthesized *via* coprecipitation method using oxalic acid and sodium hydroxide as precipitation agents. Starting from zinc acetate and europium acetate, nanopowders were obtained by coprecipitation with oxalic acid. ZnO based nanostars were synthesized by coprecipitation of Zn^{2+} and Eu^{3+} with hydroxide ions (HO^-), when zinc chloride and europium acetate were used as reagents. The structure and morphology of the as-prepared ZnO nanopowders and nanostars were investigated by X-ray diffraction and electron microscopy. Only würtzite structure of ZnO was identified in all the samples based on ZnO. Transmission electron microscopy (TEM) investigations have shown an average particle/crystallite size range from 23 to 29 nm and polyhedral and spherical morphology with tendency to form aggregates for nanopowders. Cytotoxicity tests on MG-63 cell lines was also performed. Photocatalytic activity of ZnO nanopowders have reached higher values compared to ZnO nanostars. The photocatalytic test indicates that the ZnO nanopowders have better activity than the nanostars, most probably because of the higher specific surface. Doping the ZnO with Eu_2O_3 does not seem to alter it in a decisive manner. The toxicity results indicated that ZnO nanoparticles (NPs) high toxicity on tumoral cells is also induced by particle size and, consequently, the dissolution of Zn^{2+} ions is dependent on the size of the particles, increasing with the particles size.

Keywords: ZnO nanopowders, ZnO nanostars, cytotoxicity, TEM, photoluminescence activity.

Introduction

ZnO nanoparticles (NPs) are one of the most widely used nanomaterials because of their physical and chemical properties. Due to its good electrical, optical and chemical properties, which lead to a wide range of applications, ZnO powders are often used for: photoluminescence [1], antimicrobial, catalytic [2, 3], semi-conducting, and magnetic properties [4]. Therefore, it is extremely used in personal care products [5, 6], sunscreens, paints, electronic materials, rubber manufacture, food additives, and medicine [7–10].

Several techniques such as sol–gel route [11, 12], microwave-assisted synthesis [13], hydrothermal [14], solvothermal [15], sputtering [16], reactive thermal evaporation, and precipitation [17, 18], spray pyrolysis [19, 20], pulsed laser deposition [21] method have been developed to fabricate the ZnO NPs. There is a large variety of shape in which nanostructured ZnO materials could be obtained such as powders [22, 23], nanoparticles [24], belts, nanowires [25], nanostars [26], rods [27–29], tetrapods [30, 31], flowers [32], spheres [33, 34], simple or doped [35, 36] and therefore, correspondingly, a large number of possible synthesis methods [37]. The synthesis of semiconductor nanostructures with controlled characteristics, such as orientation, density and crystalline morphology is an important aspect of modern nanoscale science and technology. Among the most studied II–IV semiconductors, ZnO has been the most suitable candidate for rear earth doping due to its wideband-gap (3.37 eV), and a large exciton binding energy (60 MeV), at room temperature [38].

Nano-sized ZnO presents exclusive characteristics that may vary a lot from bulk-sized ZnO. As the particle size of ZnO decreases, its transparency to visible light and chemical reactivity increases, despite micro-sized ZnO that exhibits high opacity and low reactivity. These features are related to high proportion of atoms on the surface of nano-sized materials in comparison with bulk-sized ones. Thereby, ZnO NPs have been used in such products where transparency or great reactivity is required.

ZnO is also known as a good photo-catalyst [39] for the degradation of several environmental contaminants due to its high photosensitivity, stability, and large band gap. ZnO offers low cost, mild reaction conditions, high photochemical reactivity, while using the sun light. ZnO can absorb UV light with the wavelength about 385 nm. For higher photocatalytic efficiency, the photocatalyst such as ZnO should absorb not only UV but also visible light considering that visible light accounts for 45% of energy in the solar radiation while UV light less than 10% [40]. In order to absorb visible light band gap of ZnO has to be narrowed or split into several subgaps, which can be achieved by doping chemical elements having high photocatalytic properties.

Despite many advantages in the wide applications of ZnO particles, nanomaterials may cause serious environmental and health problems [41–44], and as a consequence the risk of human exposure increases [45, 47]. The high reactivity of ZnO NPs may increase biological responses such as cellular uptake and delivery efficiency. Many studies on ZnO NPs toxicity were performed of different cell lines [2, 47–50], as well as in animal models [51–53].

In the present study, ZnO nanopowders and nanostars were synthesized by coprecipitation in presence of oxalic acid and sodium hydroxide. Based on toxicological aspects of bionanotechnology in relation to the presence of nanoscale entities in the human body and the consequences of transporting and interacting with tissues and organs [43], the sol–gel synthesized ZnO samples were followed by powder characterization in terms of structure, composition and morphology, through thermal analysis (TA), X-ray diffraction analysis (XRD), scanning electron microscopy (SEM) and transmission electron microscopy (TEM), respectively photoluminescence and UV–VIS analysis have been done.

The best photocatalytic activity was obtained for ZnO nanopowders doped with 3% Eu_2O_3 and for undoped ZnO nanostars. The study included an evaluation of the interaction between NPs and cell culture and a research of the influence of NPs on cell viability by using the lactate dehydrogenase method. The results indicated that exposure to ZnO NPs resulted in a concentration and time dependent increase in lactate dehydrogenase (LDH) leakage [44]. By comparing all synthesized ZnO powders, our toxicity results indicated that ZnO NPs high toxicity on tumoral cells is also induced by particle size and as a consequence, the dissolution of Zn^{2+} ions is dependent on the size of the particles, increasing with the size of the particles [54, 55].

Materials and Methods

Sample preparation

In this paper, undoped and ZnO doped with europium nanopowders and nanostars were synthesized by coprecipitation method, using as precipitation agents oxalic acid and sodium hydroxide, respectively. All reagents used are provided by Sigma-Aldrich. In order to obtain Eu-doped ZnO nanopowders, 6.56 g zinc acetate (0.0357 moles) were dissolved in 25 mL of distilled water, under magnetic stirring, and then 1%, 3% and 5% europium acetate was added. The resulting solution was added to a solution of 0.02 moles oxalic acid in 7.5 mL ethanol and 2.5 mL distilled water. After one hour of stirring at room temperature, a white precipitate of Zn and Eu oxalates was obtained. The resulting precipitate was filtered, washed with distilled water several times and dried in oven at 80^0C, for 12 hours. Finally, the dry powders were calcined at 450^0C, three hours in air.

Undoped and doped with europium ZnO nanostars were prepared by dissolving 5 g zinc chloride in 125 mL distilled water, under magnetic stirring, at 70^0C and, then adding 1%, 3% and 5% europium acetate. The as-obtained solutions were added to an alkaline solution prepared from 14.69 g NaOH dissolved in 125 mL distilled water. After 40 minutes stirring, a white precipitate of Zn and Eu hydroxides was obtained. The resulting precipitate was washed with distilled water and dried in oven at 80^0C. The calcination was performed at 400^0C.

Materials characterization

The powders were characterized by using XRD, SEM, high-resolution transmission electron microscopy (HRTEM) with selected area electron diffraction (SAED) and UV–VIS spectrophotometry. X-ray diffraction analysis were performed using an X-ray diffractometer PANalytical Empyrean, which uses a characteristic X-ray beam Cu Kα1 (λ=1.540598 Å), equipped with a hybrid monochromator 2xGe (220) for Cu and a detector with PIXcell 3D. The analyses were performed using the Bragg–Brentano geometry for the angles 2θ=20–80°. The morphology of the ZnO samples was analyzed using scanning electron microscopy and transmission electron microscopy. The SEM analysis was carried out by using a Quanta Inspect F microscope from FEI Company with field emission gun (FEG) and a 1.2 nm resolution, equipped with an energy-dispersive X-ray spectrometer (EDXS) with a resolution at Mn Kα of 133 eV.

The bright field (TEM) and high resolution (HRTEM) images coupled with SAED spectra were obtained using a Tecnai G2 F30 S-TWIN transmission electron microscope (FEI, the Nederland's), equipped with a STEM/HAADF detector, EDAX spectrometer (for energy dispersive X-ray analysis) and Gatan EELS spectrometer (for electron energy loss spectroscopy). The microscope operates at an acceleration voltage of 300 kV (Shottky field emitter) with a TEM point resolution of 2 Å and a TEM line resolution of 1 Å. Highlighting microscopic morphology and viability of MG-63 cell line was performed using the LDH. Analysis was performed on *in vitro* culture of human bone carcinoma (MG-63). Cell viability was measured using MAX Filter F5 Multi-Mode Microplate Reader (Molecular Devices, Sunnyvale, CA), according to the protocol of the kit Cell Titer 96, aqueous non-radioactive cell proliferation assay (Promega, Madison, WI, USA). Confluence 24 hours later after seeding the plates, a monolayer of MG-63 line was at a confluence approximately 70–80%. The solutions prepared for testing on cells were of concentration 1 mg/mL and incubated for 24 hours. Endothelial cells from MG-63 line were cultured in 6-well plates, with a seeding density of 75 000 cells/well in the presence of different biomaterials. After incubation for 24 hours with the material of interest, the supernatants were taken for measurements of LDH. An aliquot of 50 µL was transferred to 96-well plate. After the transfer, reagents were added, according to the following protocol: 50 µL solution 1 was added and incubated at room temperature in the dark for 30 minutes. A volume of 50 µL solution 2 was added and after that, spectrophotometric measurements are made at a 450 nm wavelength. The thermal analysis of the powders was performed with a Netzsch TG 449C STA Jupiter. Samples were placed in alumina crucible and heated with 10 K/min from room temperature to 900^0C, under the flow of 20 mL/min air. Photocatalytic activity was measured on a Methylene blue solution. For the preparation of

solutions, 0.025 g of sample was suspended in 10 mL of 0.001% Methylene blue solution under magnetic stirring. The solutions were irradiated with a 125 W mercury fluorescent lamp. At regular intervals, samples were taken for measurements of absorbance using an AbleJasco V 650 spectrophotometer. The maximum absorption wavelength of Methylene blue, 660 nm, was used for calculations.

Results

Thermal analysis

In order to establish the calcination temperature to obtain Eu-doped ZnO single phase, the synthesized powders were analyzed by thermogravimetry–differential scanning calorimetry (TG-DSC) methods at temperatures in range of room temperature up to 900^0C. For the powders obtained in the presence of oxalic acid, all the samples show similar decomposition pattern, in two steps (Figure 1, a and b).

X-ray diffraction

The XRD patterns of ZnO nanopowders and nanostars calcined at 400^0C are shown in Figure 2.

The XRD analyses indicate the formation of würtzite structure as a single crystalline phase for both europium-zinc oxide nanostructures (Figure 2), in accordance with *International Center for Diffraction Data* (ICDD) file number 04-004-4531 [14]. This indicates that the dopant ions (Eu^{3+}) substitute Zn^{2+} ions in the ZnO structure.

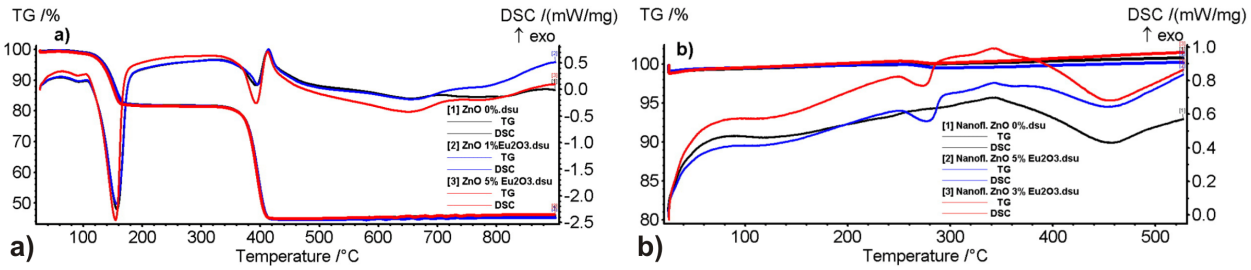

Figure 1 – ***The TG-DSC curves for ZnO nanopowders (a) and ZnO nanostars (b). TG-DSC: Thermogravimetry–differential scanning calorimetry.***

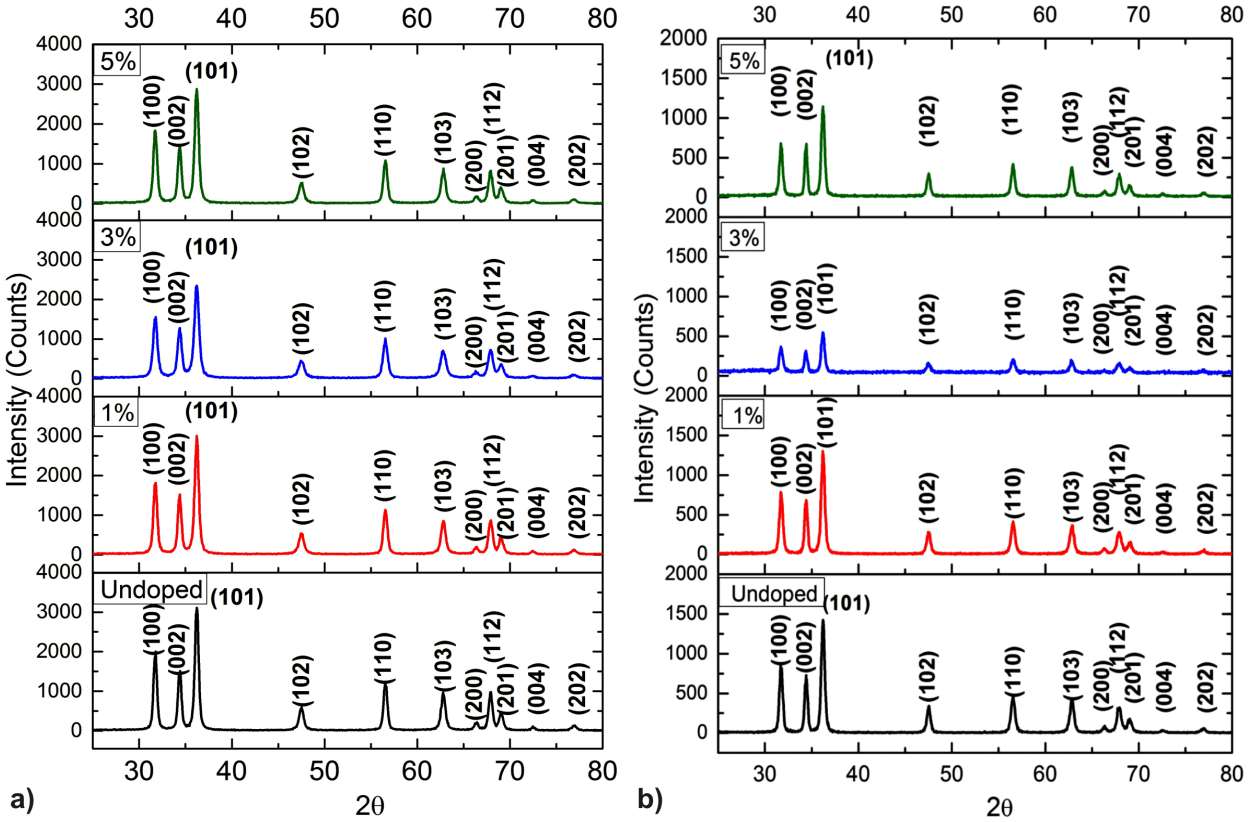

Figure 2 – ***X-ray diffraction pattern for undoped or doped with 1%, 3% and 5% Eu_2O_3 ZnO nanostructures obtained from different precursor solutions: (a) Zinc acetate; (b) Zinc chloride.***

All diffraction peaks for all samples can be assigned to the würtzite crystal structure of the zinc oxide structure, in accordance with ICDD file number 04-004-4531 [14].

In order to estimate the crystallite size variation of ZnO against Eu_2O_3 concentration, the Rietveld refinement method has been used and the results are shown in Table 1. In all cases, at the concentrations and synthesis temperatures considered, through precipitation method, nanocrystalline particles have been obtained.

Table 1 – ***Crystallites size variation values against Eu_2O_3 concentration from XRD analysis***

No.	Sample	Photocatalytic degradation rate constant [min^{-1}]
1.	ZnO_NP_0%	$8.075 \cdot 10^{-3}$
2.	ZnO_NP_1%	$7.216 \cdot 10^{-3}$
3.	ZnO_NP_3%	$8.829 \cdot 10^{-3}$
4.	ZnO_NP_5%	$7.595 \cdot 10^{-3}$
5.	ZnO NS 0%	$3.525 \cdot 10^{-3}$
6.	ZnO NS 1%	$3.037 \cdot 10^{-3}$
7.	ZnO NS 3%	$2.454 \cdot 10^{-3}$
8.	ZnO NS 5%	$3.354 \cdot 10^{-3}$

XRD: X-ray diffraction; NP: Nanopowder; NS: Nanostars.

As it can be seen, there is an increase of average nanocrystalline dimensions with increasing the Eu_2O_3 concentration. The crystallites sizes of zinc oxide nanopowders doped with 5% Eu_2O_3 reveals an increase but not exceeding the average crystallite size of undoped samples, while for ZnO nanostars could be observed values that overcome those for undoped samples.

SEM analysis

The SEM images of the ZnO and Eu-doped ZnO samples obtained starting from zinc acetate are presented in Figure 3 and, in Figure 4 are presented the SEM images for the samples synthesized from zinc chloride.

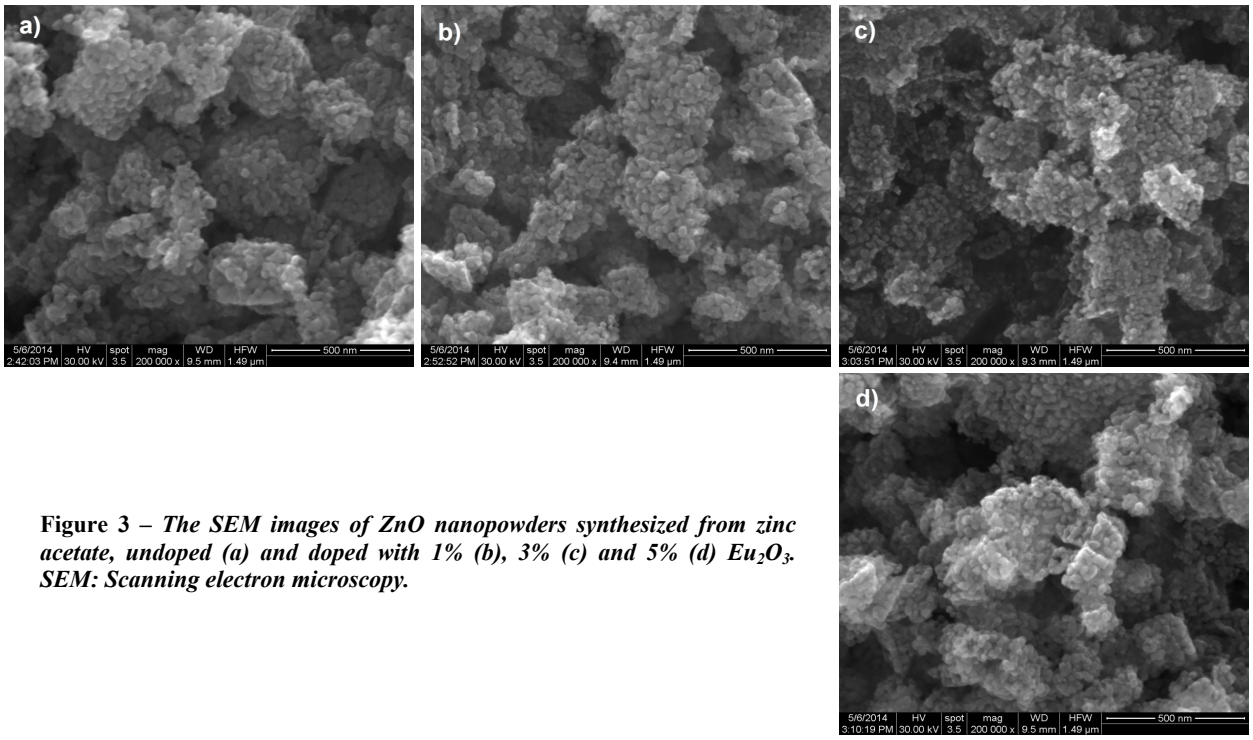

Figure 3 – ***The SEM images of ZnO nanopowders synthesized from zinc acetate, undoped (a) and doped with 1% (b), 3% (c) and 5% (d) Eu_2O_3. SEM: Scanning electron microscopy.***

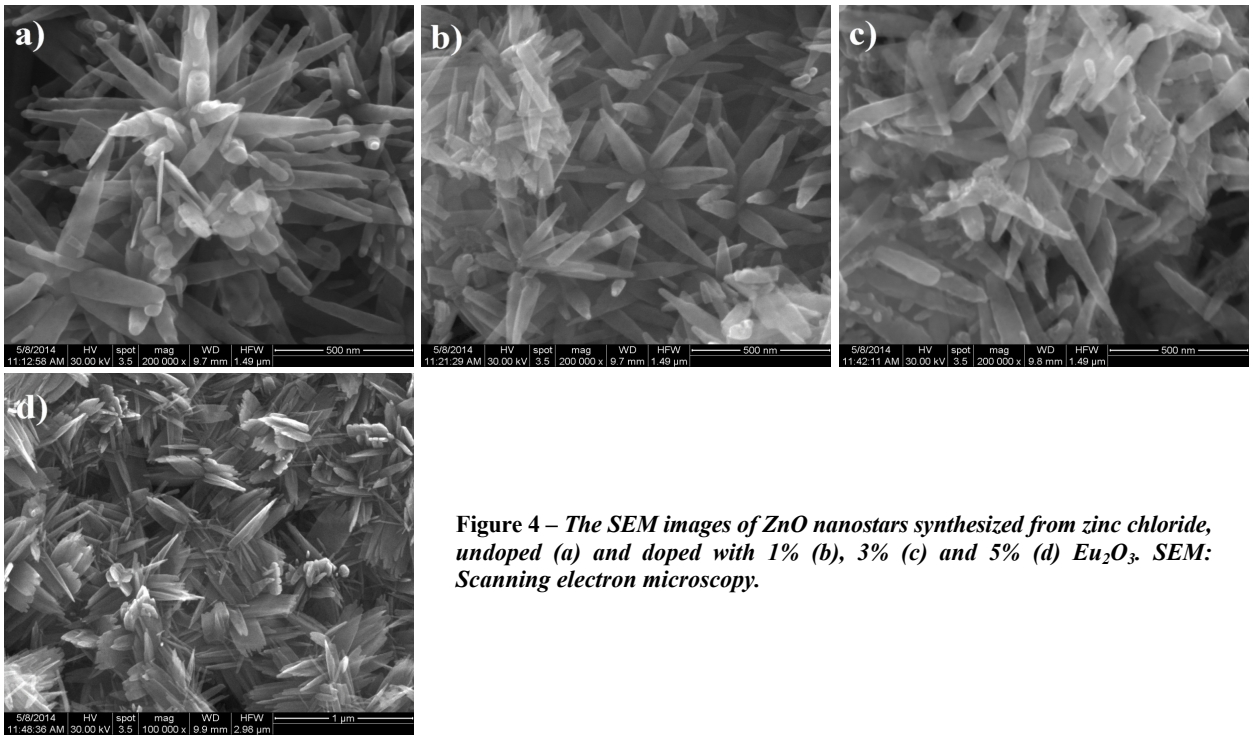

Figure 4 – ***The SEM images of ZnO nanostars synthesized from zinc chloride, undoped (a) and doped with 1% (b), 3% (c) and 5% (d) Eu_2O_3. SEM: Scanning electron microscopy.***

TEM–HRTEM analysis

The TEM, HRTEM and SAED patterns of the ZnO nanopowders obtained starting from zinc acetate are presented in Figures 5–7.

The TEM bright field images obtained on ZnO nanopowders heat treated at 450^0C, shown in Figure 5 (a, c, e and g), reveal that the nanopowder is composed from polyhedral shaped particles, with an average particle size of 23.65–29.89 nm for both types of samples, undoped or doped as well. We can observe that the only mineralogical phase identified from SAED images shown in Figure 5 (b, d, f and h) is the hexagonal form of ZnO. The histogram of size distribution for ZnO nanopowders are presented in Figure 6 (a–d), where it can be seen that the grain size distribution is monomodal for all analyzed samples. The HRTEM images obtained on nanocrystalline ZnO powders are shown in Figure 7 (a–d). We can observe very well crystallized particles that identifies orientations of ASTM ZnO hexagonal [01-080-3004] Miller indices, corresponding to interplanar distances d = [1.23820, 2.81520]. The TEM, HRTEM and SAED patterns of the ZnO nanopowders obtained starting from zinc acetate are presented in Figures 8 and 9.

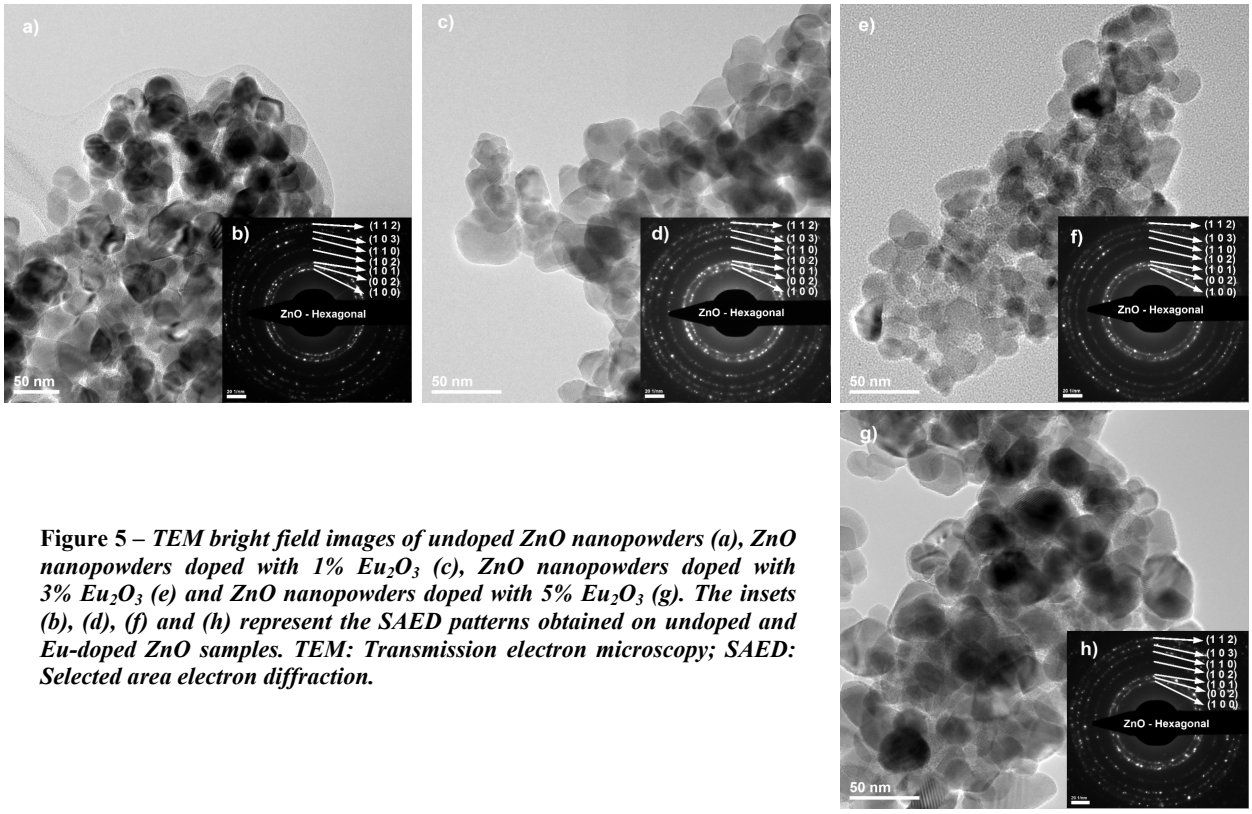

Figure 5 – ***TEM bright field images of undoped ZnO nanopowders (a), ZnO nanopowders doped with 1% Eu_2O_3 (c), ZnO nanopowders doped with 3% Eu_2O_3 (e) and ZnO nanopowders doped with 5% Eu_2O_3 (g). The insets (b), (d), (f) and (h) represent the SAED patterns obtained on undoped and Eu-doped ZnO samples. TEM: Transmission electron microscopy; SAED: Selected area electron diffraction.***

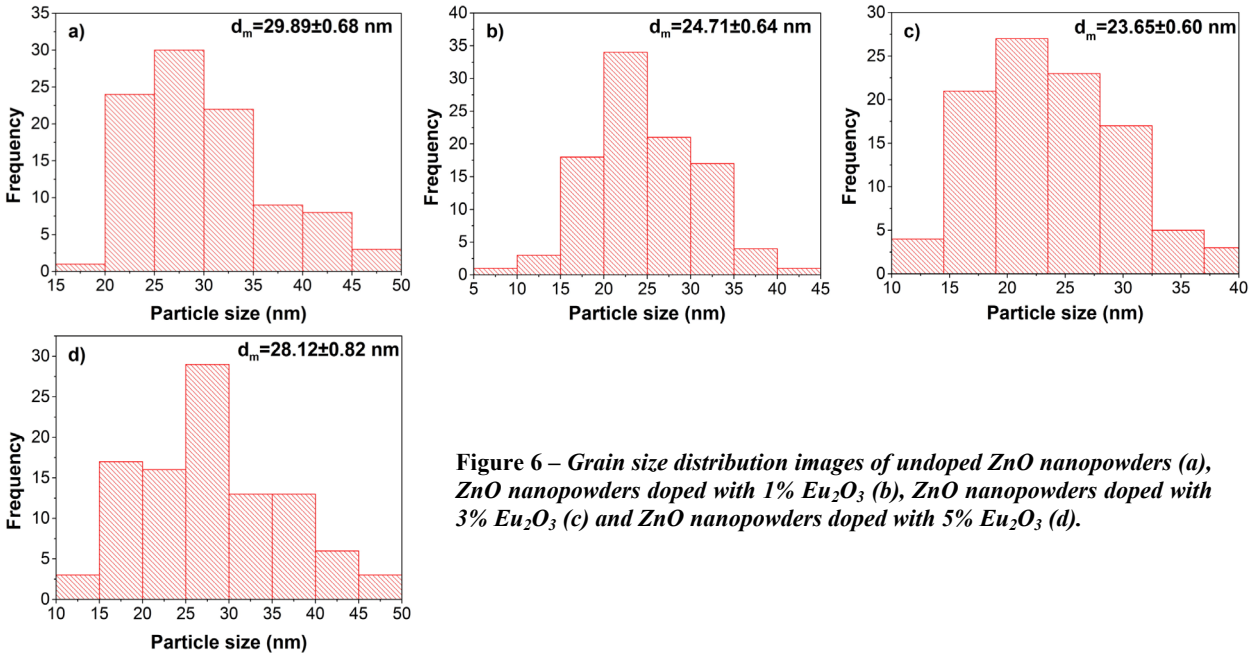

Figure 6 – ***Grain size distribution images of undoped ZnO nanopowders (a), ZnO nanopowders doped with 1% Eu_2O_3 (b), ZnO nanopowders doped with 3% Eu_2O_3 (c) and ZnO nanopowders doped with 5% Eu_2O_3 (d).***

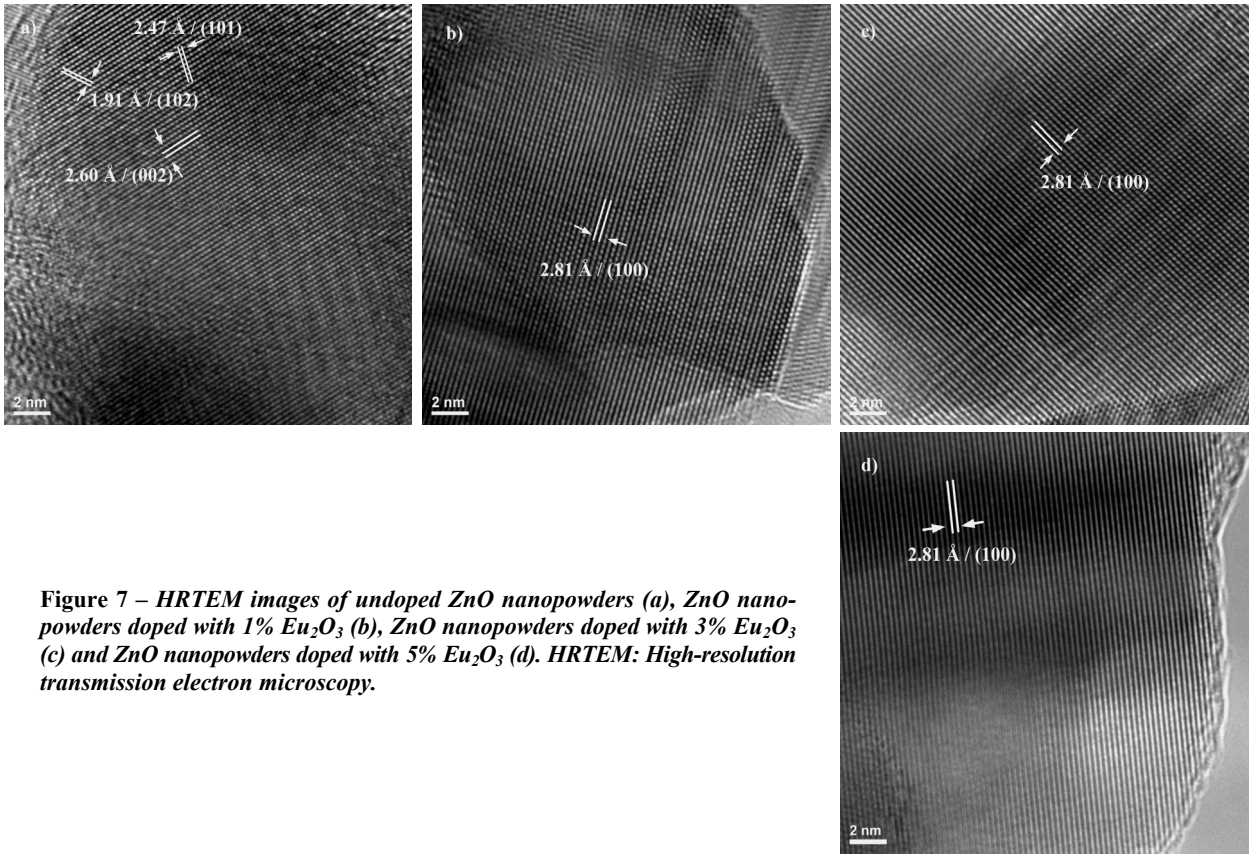

Figure 7 – ***HRTEM images of undoped ZnO nanopowders (a), ZnO nanopowders doped with 1% Eu_2O_3 (b), ZnO nanopowders doped with 3% Eu_2O_3 (c) and ZnO nanopowders doped with 5% Eu_2O_3 (d). HRTEM: High-resolution transmission electron microscopy.***

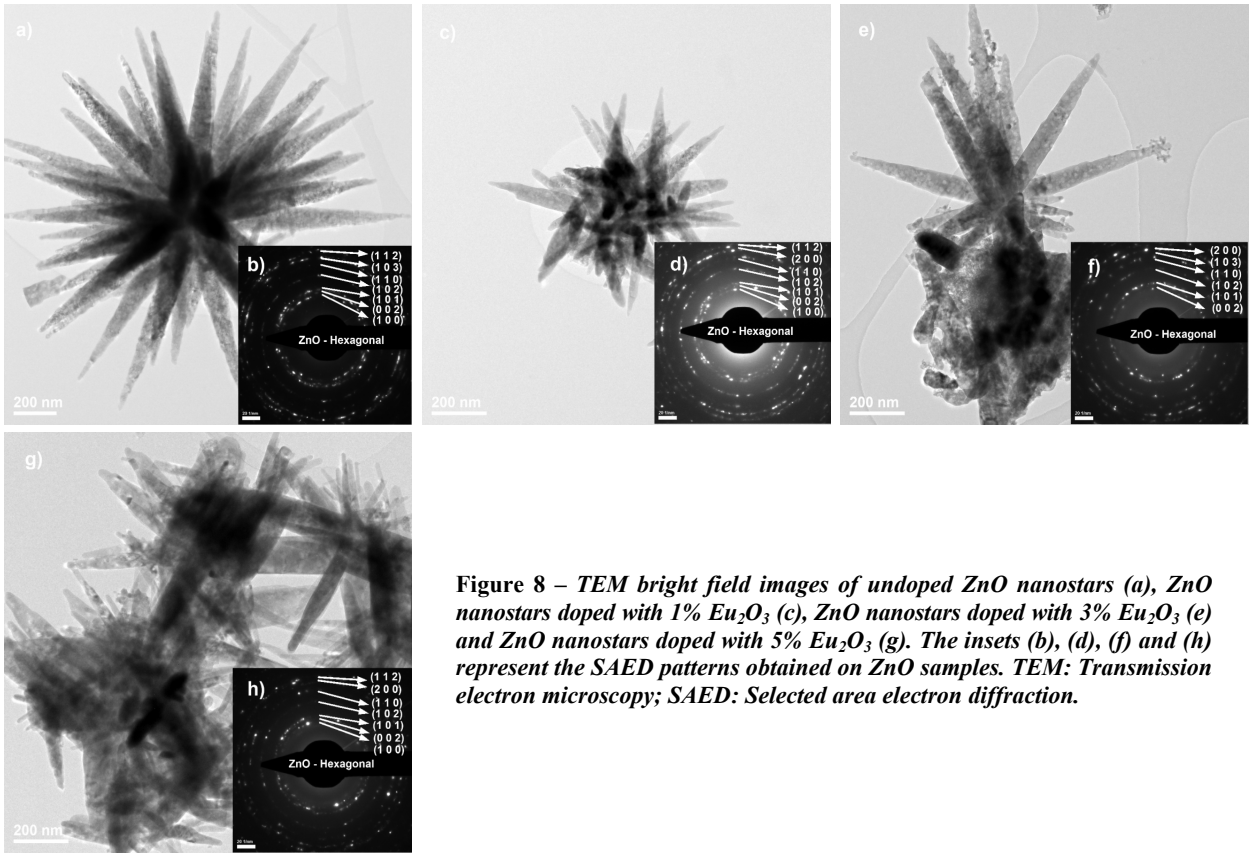

Figure 8 – ***TEM bright field images of undoped ZnO nanostars (a), ZnO nanostars doped with 1% Eu_2O_3 (c), ZnO nanostars doped with 3% Eu_2O_3 (e) and ZnO nanostars doped with 5% Eu_2O_3 (g). The insets (b), (d), (f) and (h) represent the SAED patterns obtained on ZnO samples. TEM: Transmission electron microscopy; SAED: Selected area electron diffraction.***

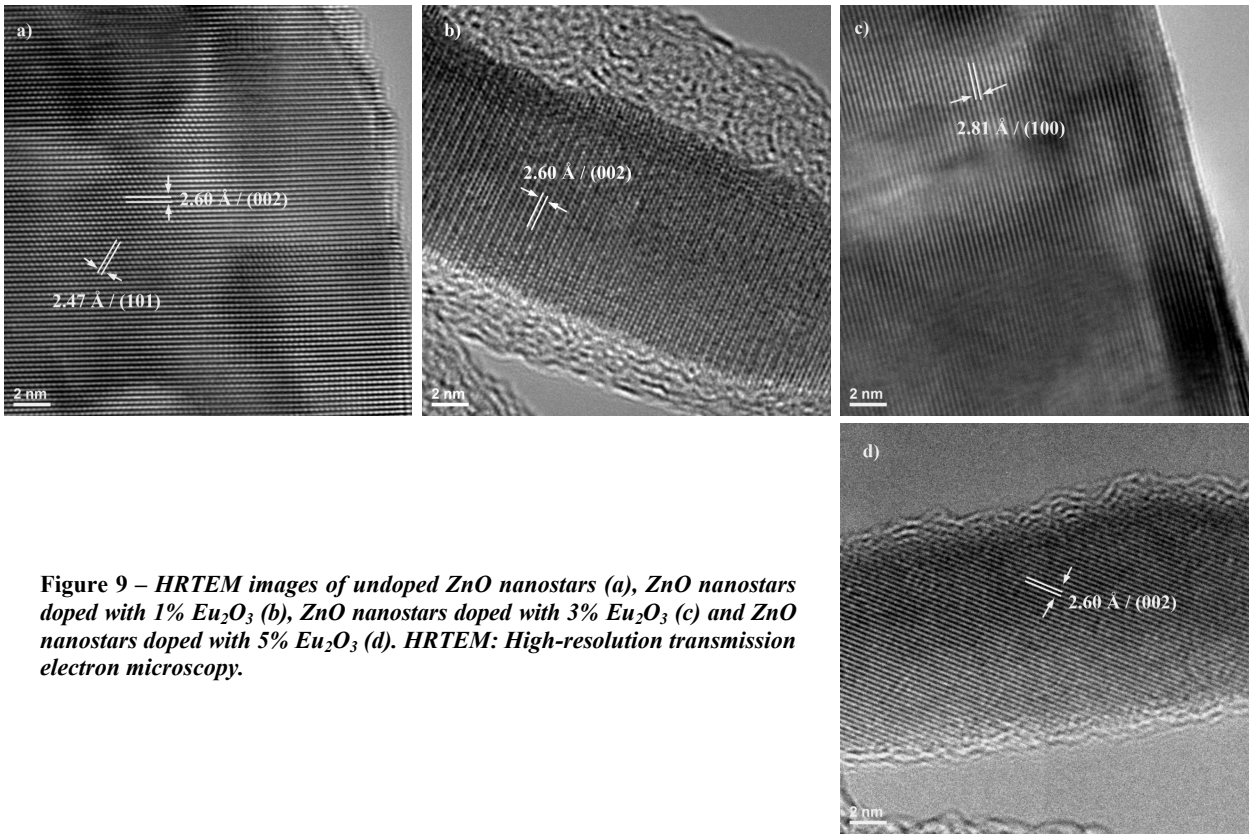

Figure 9 – ***HRTEM images of undoped ZnO nanostars (a), ZnO nanostars doped with 1% Eu_2O_3 (b), ZnO nanostars doped with 3% Eu_2O_3 (c) and ZnO nanostars doped with 5% Eu_2O_3 (d). HRTEM: High-resolution transmission electron microscopy.***

The bright field images show star-like shaped NPs, with needles that have a thickness at 100 nm, which is decreasing at the end at a thickness of about 15 nm. Nanostars morphology is highly dependent to the Eu_2O_3 addition, thus by increasing the amount or Eu the star like structure its modifying the structure. By increasing the amount of Eu_2O_3 to 5%, the structure becomes almost needle like. Selected area electron diffraction insets images present a single mineralogical phase of ZnO würtzite. From HRTEM images, very well crystallized structures could be observed, with orientations of Miller indices of (100), (002) and (101) in accordance with ASTM ZnO hexagonal [01-080-3004] [17], corresponding with interplanar distances of d=2.81 Å, d=2.6 Å and d=2.47 Å. By analyzing TEM images, we can state that the needles are single crystals.

Photoluminescence and UV–VIS properties

Figure 10a presents a comparison between the absorption spectra of Methylene blue in the presence of undoped and doped ZnO nanopowders with 1%, 3% and 5% Eu_2O_3 and undoped and doped ZnO nanostars with 1%, 3% and 5% Eu_2O_3 after irradiation for 4 hours. The results show that for ZnO nanopowder, the highest photocatalytic activity was obtained for the doped sample with 3% Eu_2O_3, followed by the undoped ZnO nanopowders. This can be due to the fact that the 3% sample has the lowest particle size, from all samples. The weakest photocatalytic activity was obtained for ZnO nanopowders doped with 1% Eu_2O_3. For ZnO nanostars samples, the best photocatalytic activity was obtained for the undoped ZnO nanostars, followed closely by the 5% Eu_2O_3 doped ZnO nanostars. The lowest photocatalytic activity was obtained for 3% Eu_2O_3 doped ZnO nanostars. Overall, the photocatalytic activity of ZnO nanopowders was more than two-folds that of the ZnO nanostars. In Figure 11, there is presented a comparison between photocatalytic activity of ZnO nanopowders (a) and ZnO nanostars (b).

Table 2 presents the rate constant calculated for the photocatalysis process in relation $ln(C_0/C)=kt$ (where C is the concentration of the Methylene blue solution at time t and C_0 is the initial concentration of the Methylene blue solution; t is time measured in minutes). As observed, the photocatalysis process follows a first order kinetics overall.

Table 2 – ***Comparison between photocatalytic degradation rate constant of ZnO nanopowders and ZnO nanostars***

No.	Sample	Photocatalytic degradation rate constant [min^{-1}]
1.	ZnO_NP_0%	$8.075 \cdot 10^{-3}$
2.	ZnO_NP_1%	$7.216 \cdot 10^{-3}$
3.	ZnO_NP_3%	$8.829 \cdot 10^{-3}$
4.	ZnO_NP_5%	$7.595 \cdot 10^{-3}$
5.	ZnO NS 0%	$3.525 \cdot 10^{-3}$
6.	ZnO NS 1%	$3.037 \cdot 10^{-3}$
7.	ZnO NS 3%	$2.454 \cdot 10^{-3}$
8.	ZnO NS 5%	$3.354 \cdot 10^{-3}$

NP: Nanopowder; NS: Nanostars.

Cytotoxicology tests on MG-63 cell lines

Cytotoxicology tests were made on MG-63 cell lines using LDH method. Analyses were performed on *in vitro* culture of human osteosarcoma cell lines MG-63, that was also used as a negative control (Figure 12).

In phase contrast microscopy images with a 20× magnification, an alteration in the immediate vicinity of

cells can be observed because of presence of the tested material. It can also be observed that the ZnO NPs are all around cells. There can still be seen viable cells, confirming the quantitative analysis with a value in range of 25–35%.

Cell morphology is completely altered, indicating low biocompatibility for undoped or doped with 1%, 3% and 5% Eu_2O_3 ZnO nanopowders and nanostars (Figures 13 and 14).

Increased toxicity of the tested materials is found both in qualitative analysis, such as phase-contrast microscopy analysis by obvious morphological alterations of treated cells, and quantitative analysis by obtaining a significant cell viability decrease (Figure 15, Table 3).

It could be observed that there is a high toxicity for all ZnO samples, indicating that the tested sample present a low biocompatibility because of the ZnO material and less because of the dopant in a small percentage in the composition. By comparing all synthesized ZnO powders, from toxicity assay it could be seen that high toxicity on tumoral cells is induced by particle size. This is due to the fact that, as stated by George *et al.* [56], ZnO toxicity is caused by the dissolution and subsequent release of the Zn^{2+} ions, that are toxic, into the aqueous culture medium. The dissolution of Zn^{2+} ions is dependent on the size of the particles, increasing with the size of the particles [57]. This effect is also seen in our case; the smallest particles were obtained for ZnO NPs and induced a lower level of cytotoxicity, whereas the obtained ZnO nanostars with larger particle size induced a higher level of cytotoxicity.

Table 3 – ***The viability values for ZnO nanostructures at a 0.5 mg***

Sample		Concentration [mg/mL]	Viability [% from control]
ZnO nanoparticles	Undoped	0.5	30
	1%	0.5	33
	3%	0.5	31
	5%	0.5	27
ZnO nanostars	Undoped	0.5	28
	1%	0.5	26
	3%	0.5	24
	5%	0.5	32

From the phase contrast microscopy images, it could be observed that on a concentration of 0.5 mg/mL, at 24 hours, viable cells are present, this also being confirmed by quantitative analysis, but it is clear that the remaining cells are affected too, as confirmed by the sudden alteration in their morphology.

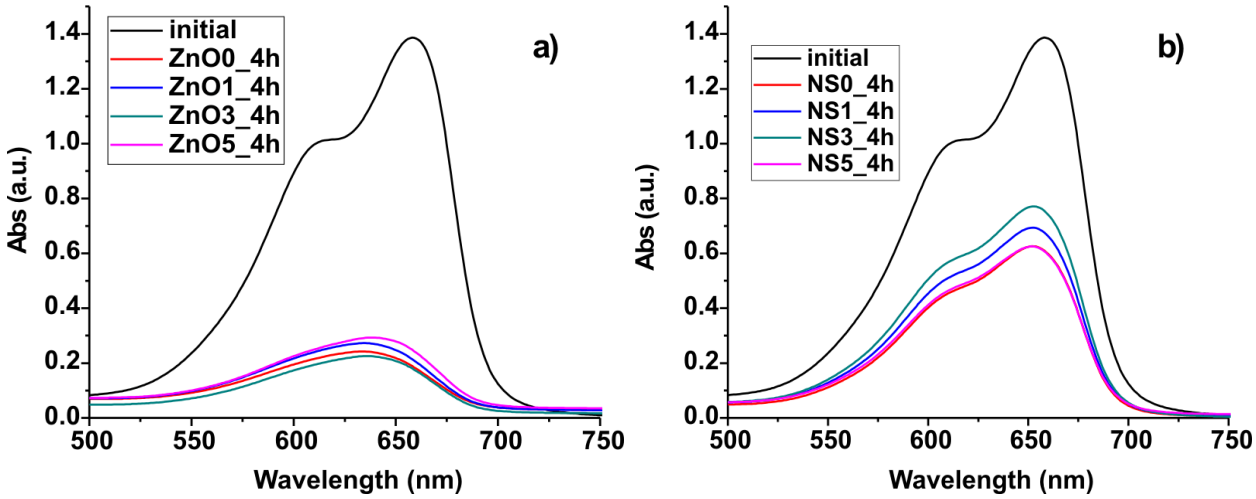

Figure 10 – ***Direct comparison between the absorption spectra of Methylene blue in the presence of undoped and doped ZnO nanopowders with 1%, 3% and 5% Eu_2O_3 (a) and undoped and doped ZnO nanostars with 1%, 3% and 5% Eu_2O_3 (b) after irradiation for four hours. NS: Nanostars.***

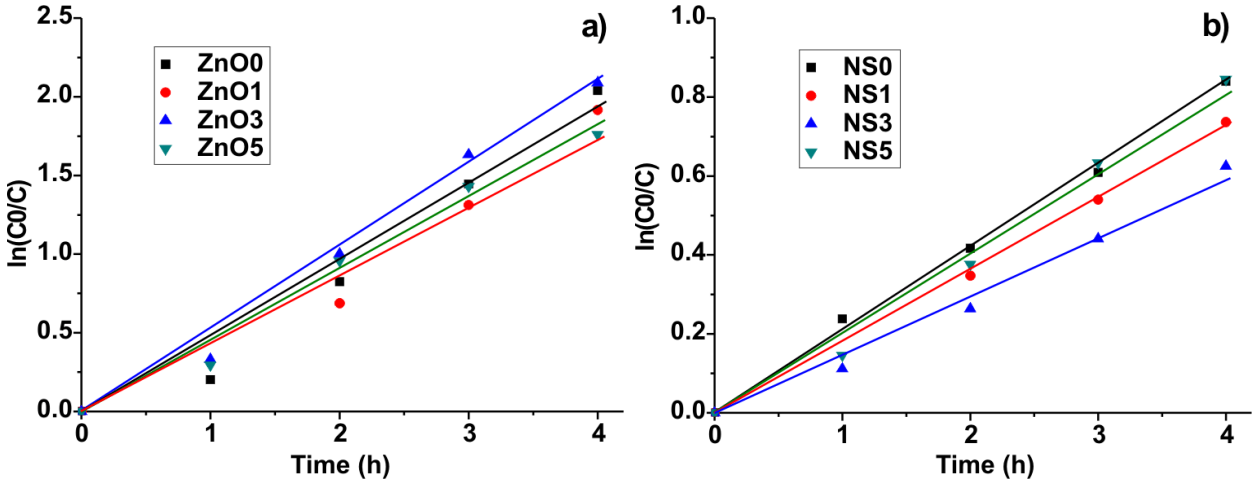

Figure 11 – ***Comparison between photocatalytic activity of ZnO nanopowders (a) and ZnO nanostars (b). NS: Nanostars.***

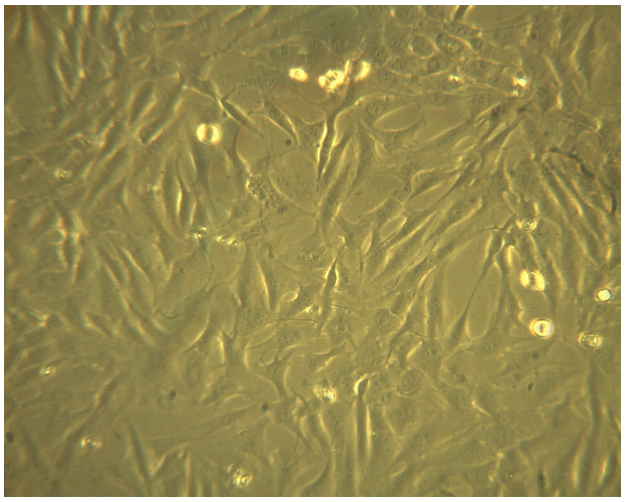

Figure 12 – ***Human osteosarcoma cell culture, phase-contrast microscopy image corresponding to untreated cells (negative control), ×200.***

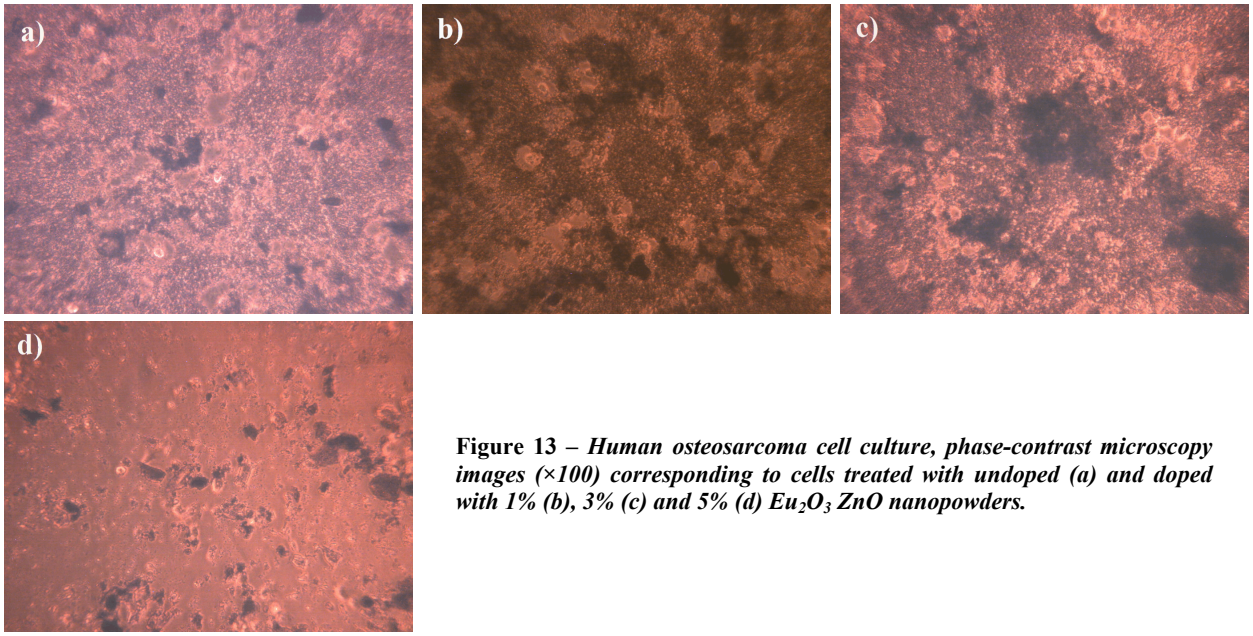

Figure 13 – ***Human osteosarcoma cell culture, phase-contrast microscopy images (×100) corresponding to cells treated with undoped (a) and doped with 1% (b), 3% (c) and 5% (d) Eu_2O_3 ZnO nanopowders.***

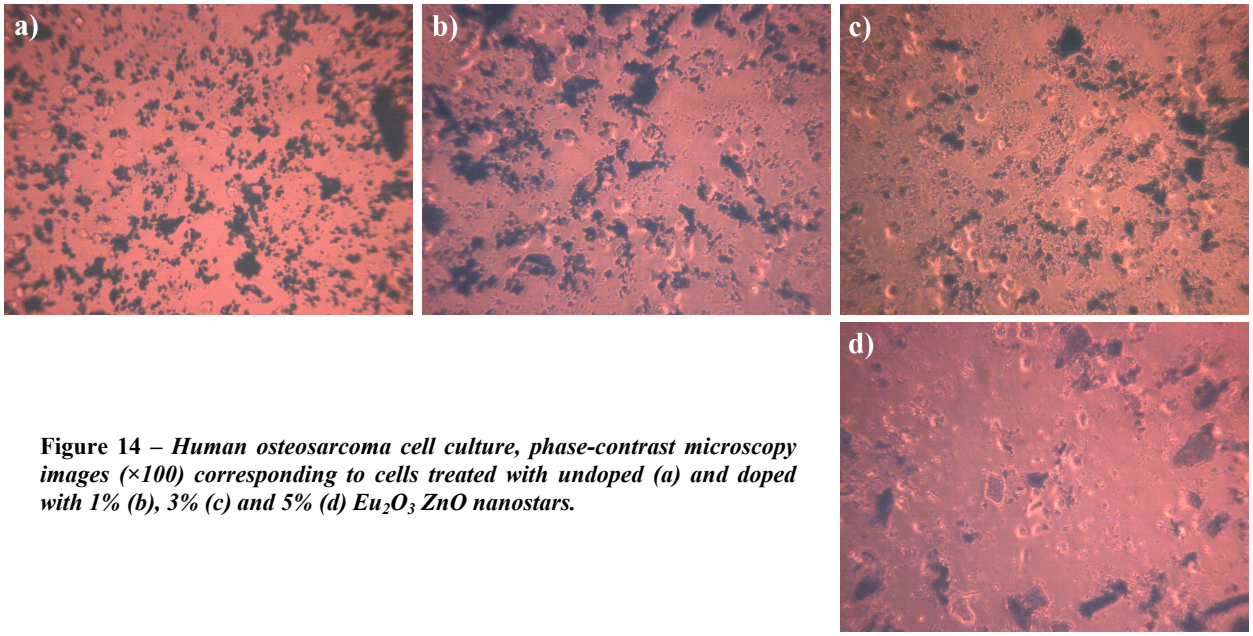

Figure 14 – ***Human osteosarcoma cell culture, phase-contrast microscopy images (×100) corresponding to cells treated with undoped (a) and doped with 1% (b), 3% (c) and 5% (d) Eu_2O_3 ZnO nanostars.***

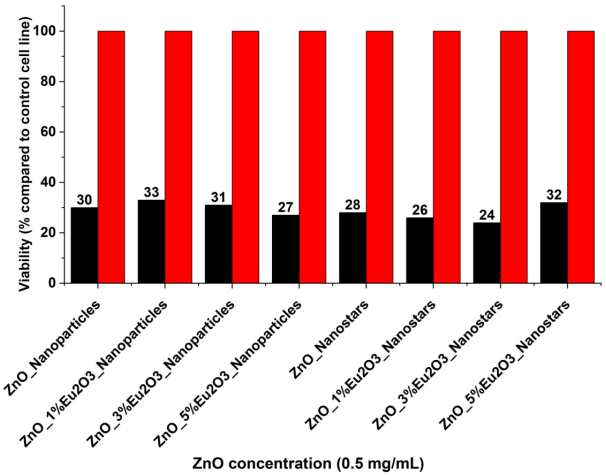

Figure 15 – ***The viability for undoped and doped with 1%, 3% and 5% Eu_2O_3 ZnO NPs and nanostars compared to control cell line.***

Discussion

According to thermal analysis, the samples exhibit two steps decomposition pattern. In the first step, up to 160^0C, the oxalates $ZnC_2O_4 \cdot xH_2O$ and $Eu_2(C_2O_4)_3 \cdot xH_2O$ lose adsorbed water, crystallization water (xH_2O) and ethanol (Figure 1a). In the interval 380–420^0C, the oxalates decompose into the corresponding oxides (ZnO and Eu_2O_3), water and CO_2. In this temperature range, the insertion of the Eu^{3+} into the crystalline lattice of ZnO also takes place. In the case of powders prepared in the presence of NaOH, the thermal analyses indicate that Eu^{3+}-doped ZnO was obtained at room temperature. The TG curves do not indicate mass losses up to 500^0C (Figure 1b).

The XRD patterns for ZnO powders reveal no significant variation of the intensity of the diffraction peaks due to the increase of Eu^{3+} concentration of Eu_2O_3 (Figure 2a). An intensity variation could be observed for ZnO nanostars patterns. The intensity values decrease from undoped samples until 3% Eu_2O_3 for doped ones, and increase at a concentration of 5% Eu_2O_3.

From the SEM images presented in Figure 3, can be seen that the nanoparticles have a uniform distribution in terms of size and show tendency to form agglomerates. The diameter of the particle decreases with the addition of Eu_2O_3 to a concentration of 3%. For samples doped with 5% Eu_2O_3 is an increase of it, but not so as to exceed the largest particle diameter in the case of undoped ZnO NPs. From the SEM images presented in Figure 4, we can clearly see that the ZnO particles are evidencing nanostructured morphology. The undoped ZnO samples that present well-defined star-like structures that become increasingly disordered with the increasing amount of Eu_2O_3 added up to 3%. For samples doped with 5% Eu_2O_3 is observed intense modification of morphology as they unravel the star-like structure and tend to acquire a platelet aspect. Nanostructures between 1–10 μm, having a needle shape with the bottom about 100 nm reaching a thickness of about 15.5 nm to the top, could be also observed in Figure 4.

When studying the photocatalytic activity, it was observed that the variation of photocatalytic activity for doped samples inside each series, although not very high, is irregular. The reason for this is that the photocatalytic activity is influenced by many other factors besides dopant percentage, such as the specific surface of the nanoparticles, the density of the surface defects, the type of defects, etc. [2, 3, 58–60].

The results from cytotoxicology tests on MG-63 cell line demonstrate that exposing the MG-63 cell line, for 24 hours, to ZnO nanopowder synthesized from zinc acetate or to ZnO nanostars synthesized from zinc chloride, undoped or doped with 1%, 3% and 5% Eu_2O_3, of a 0.5 mg/mL concentration, will increase the LDH activity with the decrease of viability at about 30%. Comparing ZnO undoped nanopowders to 1% Eu_2O_3 doped samples (Figure 14b) can be observed that the percentage of viability is only 3% lower, cell morphology is also highly altered, indicating that the toxicity of ZnO material is high. The results demonstrate that exposing MG-63 cell line, for 24 hours, to 3% doped ZnO NPs, of a 0.5 mg/mL concentration, LDH activity will increase inducing a decrease of the viability as well to 30% compared to untreated cells. For 5% Eu_2O_3 doped ZnO NPs, treated under the same conditions, the decrease in the percentage of viability is 27%, compared to untreated cells. The viability of cells treated with undoped and doped with 1%, 3% and 5% Eu_2O_3 ZnO nanostars is also reduced, indicating a low biocompatibility of this material, its cytotoxicity being similar with that of cells treated with previous materials. The results demonstrate that exposing MG-63 cell line, for 24 hours, to 3% doped ZnO nanostars, of a 0.5 mg/mL concentration, LDH activity will increase with a decrease of the viability to 28% compared to untreated cells. For 1%, 3% and 5% Eu_2O_3 doped ZnO nanostars, treated under the same conditions, the decrease in the percentage of viability is to 26%, 24% and 32% compared to untreated cells.

Conclusions

In this paper, undoped and 1%, 3% and 5% Eu^{3+}-doped ZnO nanostructures as nanopowders and nanostars, were synthesized by oxalate coprecipitation route and hydroxide coprecipitation route, respectively. X-ray diffraction spectra showed the formation of würtzite structure as a unique crystalline phase for both ZnO nanostructures. Detailed analysis has been used to determine the unit cell parameters. It has been observed that parameters indicate average crystallite size values of 18.46 nm, 17.87 nm, 15.02 nm and 17.92 nm for undoped and 1%, 3% and 5% Eu_2O_3 doped ZnO nanopowders. For undoped and 1%, 3% and 5% Eu_2O_3 doped ZnO nanostars were obtained higher values for average crystallite size, respectively 19.36 nm, 18.14 nm, 16.69 nm and 19.53 nm.

SEM and TEM analysis have indicated a granular nanostructure and a star nanostructure for the two kinds of samples, depending on the acidic or alkaline conditions of the synthesis. Polyhedral forms could be observed from ZnO nanopowders analysis. ZnO nanostars reveal a modification in morphology resulting from the quantity of dopant, getting a platelet form.

The study included an evaluation of the interaction between NPs and cell culture and a research of the

influence of nanoparticles on cell viability by using the LDH method. Cytotoxicology tests were made on *in vitro* culture of human osteosarcoma MG-63 cell lines, used as a negative control. Tests have indicated a high toxicity for all tested samples because of the ZnO material and less because of the material in a small percentage in the composition. By comparing all synthesized ZnO powders, from viability assay it could be seen that high toxicity on tumoral cells is induced by particle size. This is caused by the dissolution and subsequent release of the Zn^{2+} ions, which are toxic, into the aqueous culture medium. The dissolution of Zn^{2+} ions is dependent on the size of the particles, increasing with the size of the particles. This effect is also seen in our case, the smallest particles obtained through sol–gel method for ZnO NPs induced the lowest level of cytotoxicity, whereas the obtained ZnO nanostars with larger particle size induced the highest level of cytotoxicity. Further, the Eu_2O_3 dopant used in ZnO synthesis prove not to have a significant influence on cell toxicity.

The photocatalytic test indicates that the ZnO nanopowders have better activity than the nanostars, most probably because of the higher specific surface. The best photocatalytic activity was obtained for ZnO nanopowders doped with 3% Eu_2O_3 and for undoped ZnO nanostars. The variation of the photocatalytic activity is irregular due to many contributing factors, but doping the ZnO with Eu_2O_3 does not seem to alter it in a decisive manner.

In the future, our interest is cytotoxicity tests on epithelial cell cultures, in order to study efficiency of ZnO nanostructures in solar sunscreens.

Conflict of interests

The authors declare that they have no conflict of interests.

Acknowledgments

This work is supported by the Sectorial Operational Programme Human Resources Development, financed from the European Social Fund and by the Romanian Government under the contract number ID 134398 (KNOWLEDGE).

References

[1] Tan WK, Kawamura G, Muto H, Razak KA, Lockman Z, Matsuda A. Blue-emitting photoluminescence of rod-like and needle-like ZnO nanostructures formed by hot-water treatment of sol–gel derived coatings. J Lumin, 2015, 158:44–49.

[2] Mateos-Pedrero C, Silva H, Pacheco Tanaka DA, Liguori S, Iulianelli A, Basile A, Mendes A. CuO/ZnO catalysts for methanol steam reforming: the role of the support polarity ratio and surface area. Appl Catal B Environ, 2015, 174–175: 67–76.

[3] Kim SJ, Park DW. Preparation of ZnO nanopowders by thermal plasma and characterization of photo-catalytic property. Appl Surf Sci, 2009, 255(10):5363–5367.

[4] Husain Q. Magnetic nanoparticles as a tool for the immobilization/ stabilization of hydrolases and their applications: an overview. Biointerface Res Appl Chem, 2016, 6(6):1585–1606.

[5] Kuo CL, Wang CL, Ko HH, Hwang WS, Chang K, Li WL, Huang HH, Chang YH, Wang MC. Synthesis of zinc oxide nanocrystalline powders for cosmetic applications. Ceram Int, 2010, 36(2):693–698.

[6] Le TH, Bui AT, Le TK. The effect of Fe doping on the suppression of photocatalytic activity of ZnO nanopowder for the application in sunscreens. Powder Technol, 2014, 268: 173–176.

[7] Zhang L, Li N, Jiu H, Qi G, Huang Y. ZnO-reduced graphene oxide nanocomposites as efficient photocatalysts for photocatalytic reduction of CO_2. Ceram Int, 2015, 41(5 Pt A): 6256–6262.

[8] Rădulescu M, Andronescu E, Cirja A, Holban AM, Mogoantă L, Bălşeanu TA, Cătălin B, Neagu TP, Lascăr I, Florea DA, Grumezescu AM, Ciubuca B, Lazăr V, Chifiriuc MC, Bolocan A. Antimicrobial coatings based on zinc oxide and orange oil for improved bioactive wound dressings and other applications. Rom J Morphol Embryol, 2016, 57(1):107–114.

[9] Qayyum MA, Shah MH. Comparative assessment of essential/ toxic elemental levels in the scalp hair and nails of ovarian cancer patients and controls among Pakistani women. Biointerface Res Appl Chem, 2016, 6(6):1847–1859.

[10] Scutariu MM, Salamastrakis I, Stan CI, Nedelcu AH, Gavril LC, Costea CF, Dumitrescu AM, Sava A, Şapte E. Histopathological consequences of hyperzincemia on rat teeth. Experimental study. Rom J Morphol Embryol, 2016, 57(3):1057–1061.

[11] Arshad M, Ansari MM, Ahmed AS, Tripathi P, Ashraf SSZ, Naqvi AH, Azam A. Band gap engineering and enhanced photoluminescence of Mg doped ZnO nanoparticles synthesized by wet chemical route. J Lumin, 2015, 161:275–280.

[12] Azam A, Ahmed F, Arshi N, Chaman M, Naqvi AH. Formation and characterization of ZnO nanopowder synthesized by sol–gel method. J Alloys Compd, 2015, 496(1–2):399–402.

[13] Moghaddam FM, Saeidian H. Controlled microwave-assisted synthesis of ZnO nanopowder and its catalytic activity for O-acylation of alcohol and phenol. Mater Sci Eng B, 2007, 139(2–3):265–269.

[14] Somacescu S, Dinescu A, Stanoiu A, Simion CE, Calderon Moreno JM. Hydrothermal synthesis of ZnO–Eu_2O_3 binary oxide with straight strips morphology and sensitivity to NO_2 gas. Mater Lett, 2012, 89:219–222.

[15] Yang L, Jiang Z, Dong J, Pan A, Zhuang X. The study on crystal defects-involved energy transfer process of Eu^{3+} doped ZnO lattice. Mater Lett, 2014, 129:65–67.

[16] Barhoumi A, Leroy G, Duponchel B, Gest J, Yang L, Waldhoff N, Guermazi S. Aluminum doped ZnO thin films deposited by direct current sputtering: structural and optical properties. Superlattices Microstruct, 2015, 82:483–498.

[17] Petrović Ž, Ristić M, Musić S, Sepiol B, Peterlik H. The formation of ZnO nanoparticles from zinc gluconate. Ceram Int, 2014, 41(3 Pt B):4975–4981.

[18] Zong Y, Li Z, Wang X, Ma J, Men Y. Synthesis and high photocatalytic activity of Eu-doped ZnO nanoparticles. Ceram Int, 2014, 40(7 Pt B):10375–10382.

[19] Silva TG, Ribeiro E, Silveira E. Dark field optical imaging and photoluminescence spectra from ZnO microstructures obtained by spray pyrolysis. Phys Procedia, 2012, 28:28–32.

[20] Singh P, Kumar A, Deepak, Kaur D. Growth and characterization of ZnO nanocrystalline thin films and nanopowder *via* low-cost ultrasonic spray pyrolysis. J Cryst Growth, 2007, 306(2):303–310.

[21] Qi J, Liu W, Biswas C, Zhang G, Sun L, Wang Z, Hu X, Zhang Y. Enhanced power conversion efficiency of CdS quantum dot sensitized solar cells with ZnO nanowire arrays as the photoanodes. Opt Commun, 2015, 349:198–202.

[22] Jagannatha Reddy A, Kokila MK, Nagabhushana H, Rao JL, Shivakumara C, Nagabhushana BM, Chakradhar RPS. EPR, thermo and photoluminescence properties of ZnO nanopowders. Spectrochim Acta A Mol Biomol Spectrosc, 2011, 81(1):59–63.

[23] Cai KF, He XR, Zhang LC. Fabrication, properties and sintering of ZnO nanopowder. Mater Lett, 2008, 62(8–9):1223–1225.

[24] Orimi RL. Investigation of the effect of annealing on the photoluminescence properties of ZnO nanoparticles, synthesized at low temperature. Opt Mater, 2013, 35(3):657–660.

[25] Niu H, Zhao X, Duan L, Wang Y, Wang F, Ali A, Liu R. Influence of annealing ambient on the structure, photoluminescence and photocatalytic activity of low temperature grown ZnO nanowires. Superlattices Microstruct, 2015, 83:71–77.

[26] Li CP, Guo L, Wu ZY, Ren LR, Ai XC, Zhang JP, Lv YZ, Xu HB, Yu DP. Photoluminescence and time-resolved photoluminescence of star-shaped ZnO nanostructures. Solid State Commun, 2006, 139(7):355–359.

[27] Wang YH, Duan WJ, Wu ZL, Zheng D, Zhou XW, Zhou BY, Dai LJ, Wang YS. Enormous enhancement of ZnO nanorod photoluminescence. J Lumin, 2012, 132(8):1885–1889.

[28] Kale RB. Excitation wavelength dependent photoluminescence intensity of six faceted prismatic ZnO microrods. Optik, 2014, 125(20):6270–6273.
[29] Kim Y, Kang S. Effect of particle size on photoluminescence emission intensity in ZnO. Acta Mater, 2011, 59(8):3024–3031.
[30] Roy N, Roy A. Growth and temperature dependent photoluminescence characteristics of ZnO tetrapods. Ceram Int, 2015, 41(3 Pt A):4154–4160.
[31] Lin HF, Liao SC, Hu CT. A new approach to synthesize ZnO tetrapod-like nanoparticles with DC thermal plasma technique. J Cryst Growth, 2009, 311(5):1378–1384.
[32] Saito G, Nakasugi Y, Yamashita T, Akiyama T. Solution plasma synthesis of ZnO flowers and their photoluminescence properties. Appl Surf Sci, 2014, 290:419–424.
[33] Ren Y, Yang L, Wang L, Xu T, Wu G, Wu H. Facile synthesis, photoluminescence properties and microwave absorption enhancement of porous and hollow ZnO spheres. Powder Technol, 2015, 281:20–27.
[34] Fang TH, Chang YS, Ji LW, Prior SD, Water W, Chen KJ, Fang CF, Fang CN, Shen ST. Photoluminescence characteristics of ZnO doped with Eu^{3+} powders. J Phys Chem Solids, 2009, 70(6):1015–1018.
[35] Devi SKL, Kumar KS, Balakrishnan A. Rapid synthesis of pure and narrowly distributed Eu doped ZnO nanoparticles by solution combustion method. Mater Lett, 2011, 65(1):35–37.
[36] Fang KM, Wang ZZ, Zhang M, Wang AJ, Meng ZY, Feng JJ. Gelatin-assisted hydrothermal synthesis of single crystalline zinc oxide nanostars and their photocatalytic properties. J Colloid Interface Sci, 2013, 402:68–74.
[37] Vasile OR, Andronescu E, Ghitulica C, Vasile BS, Oprea O, Vasile E, Trusca R. Synthesis and characterization of nanostructured zinc oxide particles synthesized by the pyrosol method. J Nanopart Res, 2012, 14:1269.
[38] Pessoni HVS, Maia LJQ, Franco A Jr. Eu-doped ZnO nanoparticles prepared by the combustion reaction method: structural, photoluminescence and dielectric characterization. Mater Sci Semicond Process, 2015, 30:135–141.
[39] Pawar RC, Kim H, Lee CS. Defect-controlled growth of ZnO nanostructures using its different zinc precursors and their application for effective photodegradation. Curr Appl Phys, 2014, 14(4):621–629.
[40] Zhang H, Chen B, Jiang H, Wang C, Wang H, Wang X. A strategy for ZnO nanorod mediated multi-mode cancer treatment. Biomaterials, 2011, 32(7):1906–1914.
[41] Vandebriel RJ, De Jong WH. A review of mammalian toxicity of ZnO nanoparticles. Nanotechnol Sci Appl, 2012, 5:61–71.
[42] Xiong RD, Fang T, Yu L, Sima X, Zhu W. Effects of nano-scale TiO_2, ZnO and their bulk counterparts on zebrafish: acute toxicity, oxidative stress and oxidative damage. Sci Total Environ, 2011, 409(8):1444–1452.
[43] Roy R, Das M, Dwivedi PD. Toxicological mode of action of ZnO nanoparticles: impact on immune cells. Mol Immunol, 2015, 63(2):184–192.
[44] Seker S, Elçin AE, Yumak T, Sınağ A, Elçin YM. *In vitro* cytotoxicity of hydrothermally synthesized ZnO nanoparticles on human periodontal ligament fibroblast and mouse dermal fibroblast cells. Toxicol *In Vitro*, 2014, 28(8):1349–1358.
[45] Premanathan M, Karthikeyan K, Jeyasubramanian K, Manivannan G. Selective toxicity of ZnO nanoparticles toward Gram-positive bacteria and cancer cells by apoptosis through lipid peroxidation. Nanomedicine, 2011, 7(2):184–192.
[46] Baek M, Kim MK, Cho HJ, Lee JA, Yu J, Chung HE, Choi SJ. Factors influencing the cytotoxicity of zinc oxide nanoparticles: particle size and surface charge. J Phys Conf Ser, 2011, 304(1):012044.
[47] Wong YR, Yuan Y, Du H, Xia X. Development of high sensitivity, large frequency bandwidth ZnO-based accelerometers. Sens Actuators A Phys, 2015, 229:23–29.
[48] Darroudi M, Sabouri Z, Oskuee RK, Zak AK, Kargar H, Abd Hamid MHN. Green chemistry approach for the synthesis of ZnO nanopowders and their cytotoxic effects. Ceram Int, 2014, 40(3):4827–4831.
[49] Xia T, Kovochich M, Liong M, Mädler L, Gilbert B, Shi H, Yeh JI, Zink JI, Nel AE. Comparison of the mechanism of toxicity of zinc oxide and cerium oxide nanoparticles based on dissolution and oxidative stress properties. ACS Nano, 2008, 2(10):2121–2134.
[50] Yang H, Liu C, Yang D, Zhang H, Xi Z. Comparative study of cytotoxicity, oxidative stress and genotoxicity induced by four typical nanomaterials: the role of particle size, shape and composition. J Appl Toxicol, 2009, 29(1):69–78.
[51] Tan M, Qiu G, Ting YP. Effects of ZnO nanoparticles on wastewater treatment and their removal behavior in a membrane bioreactor. Bioresour Technol, 2015, 185:125–133.
[52] Sayes CM, Reed KL, Warheit DB. Assessing toxicity of fine and nanoparticles: comparing *in vitro* measurements to *in vivo* pulmonary toxicity profiles. Toxicol Sci, 2007, 97(1):163–180.
[53] Wang B, Feng W, Wang M, Wang T, Gu Y, Zhu M, Ouyang H, Shi J, Zhang F, Zhao Y, Chai Z, Wang H, Wang J. Acute toxicological impact of nano- and submicro-scaled zinc oxide powder on healthy adult mice. J Nanopart Res, 2008, 10(2): 263–276.
[54] Meulenkamp EA. Size dependence of the dissolution of ZnO nanoparticles. J Phys Chem B, 1998, 102(40):7764–7769.
[55] Aboulaich A, Tilmaciu CM, Merlin C, Mercier C, Guilloteau H, Medjahdi G, Schneider R. Physicochemical properties and cellular toxicity of (poly)aminoalkoxysilanes-functionalized ZnO quantum dots. Nanotechnology, 2012, 23(33):335101.
[56] George S, Pokhrel S, Xia T, Gilbert B, Ji Z, Schowalter M, Rosenauer A, Damoiseaux R, Bradley KA, Mädler L, Nel AE. Use of a rapid cytotoxicity screening approach to engineer a safer zinc oxide nanoparticle through iron doping. ACS Nano, 2010, 4(1):15–29.
[57] van Dijken A, Meulenkamp EA, Vanmaekelbergh D, Meijerink A. The kinetics of the radiative and nonradiative processes in nanocrystalline ZnO particles upon photoexcitation. J Phys Chem B, 2000, 104(8):1715–1723.
[58] Zare M, Ghashang M, Saffar-Teluri A. BaO-ZnO nano-composite efficient catalyst for the photo-catalytic degradation of 4-chlorophenol. Biointerface Res Appl Chem, 2016, 6(1):1049–1052.
[59] Khosravian P, Ghashang M, Ghayoor H. Zinc oxide/natural-Zeolite composite nano-powders: efficient catalyst for the amoxicillin removal from wastewater. Biointerface Res Appl Chem, 2016, 6(5):1538–1540.
[60] Karami S, Foroughifar N, Khajeh-Amiri A, Pasdar H. ZnO catalyzed condensation of salicylaldehyde derivatives and malononitrile. Biointerface Res Appl Chem, 2016, 6(6):1833–1836.

Corresponding author
Ionela Andreea Neacşu, PhD Student, Eng, Faculty of Applied Chemistry and Materials Science, Politehnica University of Bucharest, 1–7 Gheorghe Polizu Street, 011061 Bucharest, Romania; Phone +4021–310 76 33, e-mail: ionela.neacsu@upb.ro

Received: January 19, 2017

Accepted: December 14, 2017